



AIAA 98-4890

**Multidisciplinary Design Optimization  
of Missile Configurations and Fin Planforms  
for Improved Performance**

D. Lesieutre, M. Dillenius, and T. Lesieutre  
Nielsen Engineering & Research, Inc.  
Mountain View, CA

**7th Symposium on Multidisciplinary  
Analysis and Optimization**  
September 2–4, 1998 / St. Louis, MO

# MULTIDISCIPLINARY DESIGN OPTIMIZATION OF MISSILE CONFIGURATIONS AND FIN PLANFORMS FOR IMPROVED PERFORMANCE

Daniel J. Lesieutre,<sup>\*</sup> Marnix F. E. Dillenius,<sup>†</sup> Teresa O. Lesieutre<sup>‡</sup>

Nielsen Engineering & Research, Inc.

Mountain View, California

## ABSTRACT

The aim of the research described herein was to develop and verify an efficient optimization-based aerodynamic / structural design tool for missile fin and configuration shape optimization. The developed software was used to design several missile fin planforms which were tested in the wind tunnel. Specifically, this paper addresses fin planform optimization for minimizing fin hinge moments, as well as aeroelastic design (flexible fin structures) for hinge moment control. The method is also capable of shape optimization of fin-body combinations with geometric constraints. The inclusion of aerodynamic performance, geometric constraints, and structural constraints within the optimization software facilitates multidisciplinary analysis and design. The results of design studies and wind tunnel tests are described.

## LIST OF SYMBOLS

AR	aspect ratio of two fins joined at root chord
$C_{NF}$	fin normal-force coefficient, $force/q_{\infty}S_{ref}$
$C_{NFS}$	fin normal-force coefficient based on fin area, $force/q_{\infty}S_{fin}$
$c_R, c_T$	root chord, tip chord
f	design objective
g	equality constraint
h	inequality constraint
IP	Index of Performance (cost function)
$M_{\infty}$	Mach number
$q_{\infty}$	freestream dynamic pressure
$S_{fin}$	exposed planform area of one fin
$S_{ref}$	reference area, body cross-sectional area
s	exposed fin span
t	fin thickness
$x_{CP}/c_R$	fin axial center of pressure
$x_{HL}$	fin hinge line location aft of fin leading edge
$y_{CP}/s$	fin spanwise center of pressure
$\alpha$	body angle of attack, degrees
$\delta$	fin deflection angle, degrees
$\phi_f$	fin polar angle location, $0^{\circ}$ = horizontal, $90^{\circ}$ = windward meridian, $-90^{\circ}$ = leeward meridian
$\lambda$	fin taper ratio, $c_T/c_R$

<sup>\*</sup> Senior Research Engineer, Senior Member

<sup>†</sup> President, Associate Fellow

<sup>‡</sup> Research Engineer, Member

Copyright ©1998 by Nielsen Engineering & Research, Inc.

Published by the American Institute of Aeronautics and Astronautics, Inc. with permission.

## BACKGROUND

This paper describes recent research performed by Nielsen Engineering & Research<sup>1,2,3</sup> aimed at developing practical methods for missile control fin design and for missile configuration shape optimization. Some background information is presented which describes the importance and difficulties of predicting and designing efficient control fins. This is followed by a description of the technical approach and design code developed. Results from the design code and wind tunnel tests are presented.

Missile control fins have been, and are arguably still, the most efficient means of controlling a tactical missile and guiding it to a target. They can efficiently generate the required maneuvering force either by a direct action near the center of gravity, as in a mid-wing control missile, or through rotation of the missile to higher  $\alpha$ , as in canard or tail control missiles. Affecting all of these aerodynamically controlled configurations are the sizing and power requirements of the control surface actuators. Other means of control, such as thrust vector control and control jets are also important to high performance missiles. Thrust vector control can improve both the initial engagement of a threat, including engagement of a rear target, and the end game maneuvering (if thrust is still available). Control jets, depending on placement, can be utilized to translate or rotate a missile. Both thrust vectoring and control jets provide fast response and also provide control at high altitudes where aerodynamic control becomes ineffective. Lacau<sup>4</sup> details the advantages and disadvantages of different missile control configurations.

The primary effects of control fins on missile system design are the available maneuvering force and the time response associated with maneuvering. In terms of subsystem design, the control fins determine the actuator sizing. The actuators influence the missile weight directly through their size and power requirements. Briggs<sup>5</sup> describes the performance parameters which affect control fin actuator design and size. These include frequency-response bandwidth, stall torque, rated torque, and fin deflection rate at rated torque. The stall torque is the maximum expected "worst case" applied torque felt by the actuator and is composed of the sum (multiplied by a factor of safety) of the aerodynamic hinge moment and the frictional bearing torque associated with the fin root bending moment. Rated

torque is the maximum expected applied torque (friction + aerodynamic) over a nominal flight envelope. Fin deflection rate capability must permit three axis missile control up to the structural load limit or maximum value of total normal force acting on the missile. Rated torque multiplied by deflection rate determines the power requirements of the actuator. Actuator mass is determined primarily by the power requirements and can account for 10% of the missile mass. Reductions in hinge moments can significantly reduce this mass fraction.

Current and future air-to-air missiles are being designed for internal carriage. Internal carriage sets limits on fin span due to stowage requirements. This results in fins with reduced aspect ratios. Hinge-moment coefficients typically increase for lower aspect ratio fins due to larger variations in the axial center-of-pressure travel with both load and Mach number. The reduced span results in lower bending moments thus making the frictional bearing torques small compared to the aerodynamic hinge moments.

Historically, hinge moments have always been considered in missile designs. This has been accomplished through the choice of the most beneficial location of the hinge line over the expected flight envelope. Nielsen<sup>6</sup> states that, *“It is often contended that calculations of hinge moments are not reliable because of frequent nonlinear variation of hinge-moment coefficient with control deflection and angle of attack”* (1960). This is especially true for small values of hinge moment (desired). However, Nielsen notes that, when hinge moments are small, nonlinearities are not so important. Lacau<sup>4</sup> mentions, *“Theoretical estimate of these moments is not yet possible because the control forces center of pressure cannot be calculated with the needed accuracy. Therefore, control forces and hinge moments are obtained from wind tunnel tests”* (1988). Some examples of fins developed with considerable effort by manufacturers to minimize center-of-pressure travel are reproduced from Lacau<sup>4</sup> in Figure 1.

Not much has fundamentally changed since 1960 or 1988 in regards to the prediction or estimation of hinge moments. They are highly nonlinear with respect to  $M_\infty$ ,  $\alpha$ ,  $\phi$ , and  $\delta$ , and are difficult to predict with computational methods which lack experimental empiricism. Lesieutre and Dillenius<sup>7</sup> documented and correlated the axial and spanwise fin center of pressure for fins in the Triservice experimental data base.<sup>8</sup>  $C_{NFS}$ ,  $x_{CP}/c_R$  and  $y_{CP}/s$  are nonlinear with the flow conditions and deflection angles. It was shown<sup>7</sup> that  $x_{CP}/c_R$  and  $y_{CP}/s$  correlate with  $C_{NFS}$  for undeflected fins in the absence of strong vortical effects. Figure 2 depicts the experimental  $x_{CP}/c_R$  versus  $C_{NFS}$  for Triservice FIN52 (AR = 2,  $\lambda = 1/2$ ) for  $M_\infty = 3.0$ . There are 990 data

points plotted corresponding to 11 angles of attack from  $0^\circ$  to  $45^\circ$ , 10 windward side roll angles,  $\phi_f$ , from  $0^\circ$  to  $90^\circ$ , and 9 deflection angles from  $-40^\circ$  to  $+40^\circ$ . Data for  $\delta = 0^\circ$  are shown as solid circles and correlate fairly well with  $C_{NFS}$ . There is considerable variation of  $x_{CP}/c_R$  with deflection angle: up to 14% of  $c_R$ . When lower Mach numbers are considered, this variation is even greater since the center of pressure is further forward. Much of the deflected  $x_{CP}/c_R$  variation is associated with nonlinear effects due to the fin-body gap which are extremely difficult to predict. Results for Triservice FIN42 (AR=1,  $\lambda=1/2$ ) are shown in Figure 3. Compared to FIN52, Figure 2, this lower aspect ratio fin shows more variation of  $x_{CP}/c_R$  with  $C_{NFS}$  for both zero and nonzero deflections. With deflection, the fin-body gap is physically larger for FIN42 than for FIN52 due to different root chord lengths. Aerodynamic nonlinearities such as those depicted present a strong challenge to designers of highly maneuverable missiles which operate from subsonic to hypersonic speeds.

The approach described herein<sup>1,2,3</sup> to design control fins with improved performance is a practical one which utilizes numerical optimization and nonlinear aerodynamic prediction methods. The primary goal was to design fins with improved performance over that of the initial or baseline fin. Therefore, it is not strictly necessary that the aerodynamic prediction accurately model all the nonlinearities present. However, it must estimate the relative performance of fins adequately. Promising designs were analyzed with CFD for verification prior to wind tunnel testing.

## TECHNICAL APPROACH

A numerical optimization shell has been coupled with subsonic and supersonic fast running panel method-based missile aerodynamic prediction programs which include nonlinear high angle of attack vortical effects and a structural finite element code.<sup>1,2</sup> Program OPTMIS<sup>1,2</sup> for missiles with arbitrary cross section bodies and up to two fin sections was developed under a U.S. Air Force Small Business Innovative Research (SBIR) contract. A U.S. Navy SBIR effort investigated the extension to and design of flexible composite fin structures which aeroelastically minimize hinge moments.<sup>3</sup> A description of the methodology employed follows.

### Summary of Methodologies Employed

The optimization algorithm implemented in the OPTMIS<sup>2</sup> design software is a direct search algorithm, Powell's Conjugate Directions Method.<sup>1,9,10</sup> The Nielsen Engineering & Research (NEAR) subsonic and supersonic panel method-based aerodynamic prediction modules, SUBDL<sup>11</sup> and SUPDL,<sup>12,13</sup> are employed as the aerodynamic prediction modules within the design code. The VTXCHN<sup>14</sup> methodology is used to model

circular and noncircular body shapes within the SUBDL and SUPDL modules. The structural constraints are included through the CNEVAL-FEMODS<sup>1,3</sup> module which employs automatic gridding and structural finite elements to compute displacements, stresses, fin weight, and natural mode frequencies.

For aeroelastic design studies, subiterations between the aerodynamic and structural analysis module CNEVAL-FEMODS<sup>1,3</sup> are performed to ensure a consistent load distribution and deformed fin shape. Initially, fin displacements are calculated with the flat-fin (rigid) load distribution. The fin displacements are used to define a new fin shape for the aerodynamic load calculation, and the aerodynamic loads are recalculated. Fin displacements are determined with the updated loads, and this iterative process is continued until the changes in displacements are less than a user-specified tolerance.

### Optimization Problem Formulation

The *OPTMIS*<sup>2</sup> design software minimizes an Index of Performance (cost function) which includes objectives, equality constraints, and inequality constraints. This formulation is an extension of the Sequential Unconstrained Minimization Technique (SUMT) of Fiacco and McCormick.<sup>15</sup> The SUMT formulation was enhanced so that multiple objective functions and multiple design point studies could be included. The following SUMT Index of Performance is employed:

$$IP(\mathbf{x}, \mathbf{w}) = \sum_m [\sum_i f_i(\mathbf{x}, m) / w_i] + \sum_j [h_j^2(\mathbf{x}) / w_j] + \sum_k [w_k / g_k(\mathbf{x})] \quad (1)$$

where the indices m, i, j, and k represent sums on the number of flow conditions, objectives, equality constraints, and inequality constraints, respectively. The constraint weights,  $w_j$  and  $w_k$ , are monotonically decreased during the optimization procedure. The inequality constraints  $g_k(\mathbf{x})$  add a large positive value to the IP if  $g_k(\mathbf{x})$  approaches zero. If there are no inequality constraints, the minimization problem being solved is an unconstrained minimization of  $f(\mathbf{x})$  when  $w_j$  is large. As  $w_j$  decreases toward zero, the equality constraints become important. This representation of the Index of Performance is very versatile and allows single and multiple point designs to be investigated.

In *OPTMIS*,<sup>2</sup> the index of performance formulation given by Eqn. (1) is further divided into three terms governing design objectives and constraints applicable to the fin, body, and overall configuration. The complete form of the IP is given by:

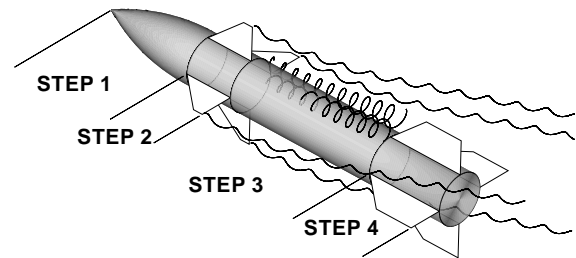
$$IP(\mathbf{x}, \mathbf{w}) = IP_{overall}(\mathbf{x}, \mathbf{w}_o) + IP_{body}(\mathbf{x}, \mathbf{w}_b) + IP_{fin_n}(\mathbf{x}, \mathbf{w}_f) \quad (2)$$

where  $IP_{overall}$ ,  $IP_{body}$ , and  $IP_{fin}$  each have the form of Eqn. (1) and correspond to overall, body, and fin objectives and constraints, respectively.  $IP_{fin}$  includes objectives and constraints for up to two fin sections. Typically, objectives are formulated with respect to aerodynamic performance variables, and constraints with respect to geometric variables.

Program *OPTMIS*<sup>2</sup> has two methods for handling the inequality constraints specified. The first is in the manner specified in Eqn. (1), through a penalty within the IP. The second is as a side constraint. If an initial feasible design is specified, then the optimization procedure will not allow a design change in a direction where an inequality constraint is violated. This is the manner in which all structural constraints computed by the CNEVAL-FEMODS<sup>1,3</sup> module are handled.

### Aerodynamic Modeling

This section gives a brief summary of the body and fin aerodynamic modeling methodologies used in the *OPTMIS* code. The NEAR nonlinear panel method-based missile aerodynamic prediction programs SUBDL<sup>11</sup> and SUPDL<sup>12,13</sup> which include models of body and fin shed vorticity at high angles of attack, as well as nonlinear shock expansion and Newtonian analyses, were chosen as appropriate aerodynamic codes for inclusion in the aerodynamic optimization tool. General descriptions of programs SUPDL and SUBDL follow. The original SUBDL and SUPDL codes modeled axisymmetric bodies. The VTXCHN code<sup>14</sup> has replaced the body model within SUBDL and SUPDL and can model circular and noncircular cross section bodies including those with chines. The aerodynamic calculation proceeds stepwise as follows: 1) VTXCHN computes the forebody loads including vortex shedding and tracking, 2) fin section loads are calculated including the effects of forebody vorticity, 3) vorticity shed from the forebody and the fin set is tracked aft including additional vortices shed from the afterbody, and 4) if a second fin set is present, steps 2 and 3 are repeated. This procedure is depicted below.



### VTXCHN Body Modeling Methodology

The aerodynamic analysis of a body by VTXCHN,<sup>14</sup> including effects of vortex shedding, comprises conformal mapping, elements of linear and slender body

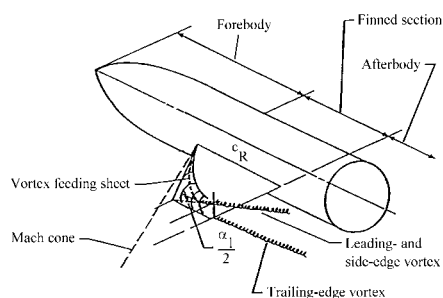
theory, and nonlinear vortical modeling. The analysis proceeds from the nose to the base. Noncircular cross sections are transformed to corresponding circles in the mapped plane. As a result, an axisymmetric body is created in the mapped space. If the actual body is axisymmetric, this step is omitted. The axisymmetric body is modeled by three-dimensional sources/sinks for linear volume effects and by two-dimensional doublets for linear upwash/sidewash effects. For subsonic flow three-dimensional point sources/sinks are used, and for supersonic flow three-dimensional line sources/sinks are used. At a cross section near the nose, velocity components are computed at points on the transformed body and transformed back to the physical plane. The circumferential pressure distribution is determined in the physical plane using the compressible Bernoulli equation. For smooth cross sectional contours, the code makes use of the Stratford separation criterion applied to the pressure distribution to determine the separation points. If the cross section has sharp corners or chine edges, vortices are positioned slightly off the body close to the corner or chine points in the crossflow plane. The locations of the shed vortices are transformed to the mapped plane. The strengths of the shed vortices are related to the imposition of a stagnation condition at the contour corner or chine points in the mapped plane. The vortices are then tracked aft to the next cross section in the mapped plane. The procedure for the first cross section is repeated. The pressure distribution calculated at the second cross section in the physical plane includes nonlinear effects of the vortices shed from the first cross section. The resulting pressure distribution is integrated to obtain the aerodynamic forces and moments. Along the body, the vortical wake is represented by a cloud of point vortices with known strengths and positions.

### Supersonic Aerodynamic Prediction Method

SUPDL<sup>12,13</sup> is a panel method-based program which together with the VTXCHN<sup>14</sup> body module can analyze an arbitrary cross section body with a maximum of two fin sections in supersonic flow. Fins may have arbitrary planform, be located off the major planes, and be attached at arbitrary angles to the body surface. The fins are modeled by supersonic panels laid out in the chordal planes of the fins. In addition, a set of panels is laid out in a shell around the body over the length of the fin root chord to account for lift carry-over. The panel method is based on the Woodward constant pressure panel solution<sup>16</sup> for modeling lift. In SUPDL this panel is designated the constant u-velocity panel because the pressure on the panel is computed using the compressible Bernoulli velocity/pressure relationship. Each panel has a control point at which the flow tangency condition is applied. On the fin, the flow tangency boundary condition includes mutual interaction

with all other constant u-velocity panels in the fin section, contributions from free stream due to angle of attack, body-induced effects (upwash), and vortical wakes from upstream fins and body flow separation. The constant u-velocity panels on the interference shell only experience the mutual interaction with the constant u-velocity panels on the fins and fin thickness effects. Effects of fin thickness can be included by thickness panels in the chordal plane of the fin. The strengths of the thickness panels are directly related to the local thickness slopes. The strengths of all of the constant u-velocity panels in a fin section are obtained from a solution of a set of simultaneous equations.

Fins can develop nonlinear leading- and side-edge separation vorticity as the angle of attack is increased. If the side edge is long (similar in length to the root chord, for example), vorticity can be generated at angles of attack as low as 5°. Along the leading edge, vorticity can be generated at supersonic speeds provided the leading edge lies aft of the Mach cone emanating from the root leading edge (a subsonic leading edge). If this is the case, the leading-edge vortex joins the side-edge vortex. The combined vortex gains strength and rises above the fin as shown in the sketch which follows. This sketch shows how SUPDL models the path of the combined leading- and side-edge vortex by locating it above the fin plane at an angle equal to one-half of the local angle of attack (as seen by the fin).



The vortical phenomena along the leading- and side-edges are accompanied by an augmentation to normal force which is nonlinear with angle of attack seen by the fin. This nonlinearity is modeled by calculating the suction distribution along the leading and side edges. In accordance with an extension<sup>17</sup> of the Polhamus suction analogy,<sup>18</sup> the suction is converted to normal force in proportion to vortex lift factors. The result is a distribution of nonlinear, additional normal force along the leading and the side edge.

Another nonlinear effect is related to nonlinear compressibility. For  $M_\infty$  in excess of approximately 2.5, the fin leading edge shock may lie close to the surfaces (usually the lower surface) of the fin. This situation can

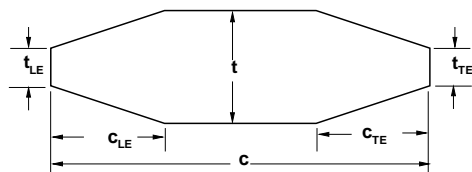
also occur at low supersonic Mach numbers if the angle of attack is high. In either case, the fin loading prediction based on the constant u-velocity panel method and the Bernoulli velocity/pressure relationship is no longer adequate. As an option, the pressures acting along chordwise strips can be calculated with nonlinear shock expansion or Newtonian theories. A unique feature is the option to include strip-on-strip interference based on the linear constant u-velocity panel solution to correct the flow angle used in either the shock expansion or Newtonian pressure calculation methods. Details can be found in References 17 and 19.

### Subsonic Aerodynamic Prediction Method

Program SUBDL<sup>11</sup> is a panel method-based program which together with the VTXCHN<sup>14</sup> body module can analyze an arbitrary cross section body with a maximum of two fin sections in subsonic flow. The addressable geometries are the same as those described for SUPDL previously. The lifting surfaces and the portions of the body spanned by the lifting surfaces are modeled with planar horseshoe vortex panels. The strengths of the lifting surface singularities are obtained from a set of linear simultaneous equations based on satisfying the flow tangency condition at a set of discrete aerodynamic control points. The horseshoe vortices on the interference shell around the body are used only to model the carryover forces between the body and fins (the body volume and angle-of-attack effects are obtained from the three-dimensional sources and doublets and conformal mapping procedure in the VTXCHN module). The nonlinear vorticity effects associated with fin edges described above for SUPDL are also modeled in SUBDL.

### Fin Structural Modeling

For fin structural modeling, five parameters for the root and five parameters for the tip define the thickness distributions. The parameters for any intermediate section are defined by linear interpolation. The generic section is a symmetric truncated double wedge with finite thicknesses at the leading and trailing edges and is illustrated in the sketch below.



The fin can be cantilevered at the root, or supported on a shaft to represent an all-movable control surface.

The fin is modeled with constant-thickness, triangular nonconforming bending elements,<sup>20</sup> with modifications to allow for anisotropy.<sup>21</sup> The meshed fin is divided into quadrilateral patches. In the simplest model, each

patch is represented by two bending elements. However, since nonconforming elements do not reproduce the proper symmetry properties for a rectangular or a square planform, there is an option to model each patch with two pairs of elements which eliminates any asymmetries. For all-movable fins, the control shaft is modeled with a beam in bending and a rod in torsion. No transverse shear effects are included, and both elements are uniform. These elements are also described in detail in Reference 22. There are three degrees of freedom per structural node: two rotations in the plane of the fin, plus a transverse displacement. For dynamic problems, consistent inertia elements from Reference 22 are used.

**Structural Constraint Evaluation.** There are two options for displacement constraints. In the first option, up to 10 upper bounds and their associated node numbers can be specified. Displacement ratios (actual/allowable) are calculated at the specified nodes; if any ratio is greater than unity, the number of violated displacement constraints is incremented, and the node number and displacement ratio are recorded. In the second option, only a single upper bound for the maximum absolute value of any displacement is specified. If this bound is exceeded, then the number of violated displacement constraints is set to unity, and the node number and displacement ratio are recorded. For the stress constraint, the maximum value of the von Mises bending stress is found. If this value exceeds the allowable, the constraint-violation flag is set to unity and the associated node number and stress ratio are recorded. Up to five lower-bound frequency constraints can be imposed by specifying the lower bounds and their mode numbers. A frequency constraint is considered violated when the frequency for any specified mode becomes less than its bound. The number of violated constraints and the corresponding mode numbers and frequency ratios are recorded. For the weight constraint, the weight of the initial design is saved. The weight of each subsequent design is ratioed to this initial weight.

## RESULTS

This section describes results including fin planform design studies, wind tunnel tests, verification of aerodynamic performance prediction, and aeroelastic fin design. Additional design studies are described in References 1, 2, and 3.

### Fin Planform Optimization Design Studies

Descriptions of two fin planform optimization designs which were tested in the Lockheed-Martin High Speed Wind Tunnel in Dallas, TX, are given below. For the fin designs tested in the wind tunnel, four (4) small span fins, FIN1 - FIN4, with exposed span of 0.72 diameters, and two (2) large span fins, FIN5 and FIN6, with

exposed span of 1.4 diameters were tested. FIN1 was the small span trapezoidal reference fin used to start the design optimization for FIN2, FIN3, and FIN4. FIN6 was the large span trapezoidal reference fin used to start the design optimization for FIN5. The design studies for FIN3 and FIN5 are described in this paper. Further details can be found in Reference 1.

FIN3 and FIN5 were designed using *OPTMIS*<sup>2</sup> to minimize the fin axial center-of-pressure travel from subsonic to supersonic flow. The fin normal force based on fin area was to be maintained. To achieve this objective, the ratio  $|x_{CP2} - x_{CP1}|/|C_{NF2} - C_{NF1}|$  was minimized. The subscript "2" refers to the supersonic design flow condition, and the subscript "1" refers to the subsonic design flow condition. This design objective also tends to give a flat  $x_{CP}$  response with increasing fin normal force. The design flow conditions were:  $(M_\infty, \alpha) = (0.5, 2^\circ), (2.0, 15^\circ)$ . For the reference fins, the low  $M_\infty$  number, low  $\alpha$  design condition gave a center of pressure forward on the fin, whereas the supersonic Mach number, high angle-of-attack condition gave an aft center-of-pressure location. The design objective was to minimize this center-of-pressure travel. The design variables were third-order Chebyshev polynomials describing the leading- and trailing-edge shapes. The resulting geometries of FIN3 and FIN5 are shown in Figures 4 and 10, respectively.

### Wind Tunnel Test Description

The fin planforms described above were tested in the Lockheed-Martin High Speed Wind Tunnel in Dallas, TX, during the period March 3 - 8, 1997. Existing test hardware consisting of a body with fin strain-gage balances was utilized. The model consisted of a two-caliber tangent ogive nose and a cylindrical body 5.2 calibers long. A pair of fin balances were positioned 3.4 diameters aft of the nose tip. Figures 4, 6, and 10 depict the fins described herein. All tests were conducted with identical fins on the left and right balances to insure symmetry. The three-component outputs for the fins, (1) normal force, (2) root-bending moment, and (3) hinge moment, were the only model data collected. The internal structure of the body permitted mounting the fins at deflection angles from  $-20^\circ$  to  $+20^\circ$  at  $5^\circ$  intervals. The fin force,  $C_{NF}$ , and moment data,  $C_{HM}$  and  $C_{BM}$ , were reduced to provide fin axial and spanwise center-of-pressure locations,  $x_{CP}/c_R$  and  $y_{CP}/s$ , respectively. The tests included Mach numbers of 0.5, 1.5, 2.0, and 3.0. The angle of attack range was  $-12^\circ$  to  $22^\circ$ , and fin deflection angles of  $0^\circ$  and  $20^\circ$  were tested.

### Prediction Verification for Reference FIN1

The predicted and measured aerodynamic performance of the small span reference fin FIN1 is shown in Figures 4 and 5. The variation of fin normal force  $C_{NFS}$

and fin axial center of pressure  $x_{CP}/c_R$  with  $\alpha$  are shown for  $M_\infty = 0.5$  and  $2.0$  and for  $\delta = 0^\circ$  and  $20^\circ$ . Experimental data are shown as open symbols. Predicted results from *OPTMIS*<sup>2</sup> are shown as solid symbols with solid lines, and results from the NASA OVERFLOW Navier-Stokes solver<sup>22</sup> (zero deflection only) are shown as solid symbols with dashed lines.

The comparison of the measured and predicted  $C_{NFS}$  for  $\delta = 0^\circ$  are in good agreement for both Mach numbers. *OPTMIS* slightly overpredicts  $C_{NFS}$  at  $M_\infty = 2.0$  and  $\alpha = 20^\circ$ . OVERFLOW slightly underpredicts  $C_{NFS}$  at  $M_\infty = 0.5$  and  $\alpha = 20^\circ$ . The axial center-of-pressure location is also predicted well for the  $\delta = 0^\circ$  conditions. All design studies have been performed at  $\delta = 0^\circ$ . The predicted aerodynamic results for  $\delta = 20^\circ$  are not in as good an agreement with the experiment. For  $M_\infty = 0.5$ , the *OPTMIS* results for  $C_{NFS}$  agree fairly well at low angles of attack but do not have the correct stall behavior as angle of attack increases. The predicted axial center of pressure is forward of the experimental result for angles of attack above  $10^\circ$ . This is most likely due to inadequate modeling in *OPTMIS* of the gap between the deflected fin and the body which changes the fin loads near the root chord leading or trailing edge. The subsonic prediction module, SUBDL, currently models the effects of deflection through the boundary conditions and not through geometric deflection of the fin. This accounts for both the overprediction of normal force and the forward location of the center of pressure. The deflected results for the supersonic Mach number,  $M_\infty = 2.0$ , show the opposite trend. The normal force is underpredicted in this case. The supersonic prediction module, SUPDL, does model deflection effects through geometric deflection of the fin. However, the nonlinear flow field (local Mach number and local dynamic pressure variations) present behind the nose bow shock can be important when the fin is close to the nose. For this forward fin position, the flow field can vary significantly circumferentially around the body. For large deflections this places the leading and trailing edges in different local flow fields. The local flow fields behind the bow shocks close to the body surface can only be predicted well by Euler or Navier-Stokes flow solvers. The panel method-based programs are not capable of predicting these local flow conditions. However, corrections based on CFD calculations could be included. In spite of the above, the axial center of pressure is predicted well by *OPTMIS*.

### Prediction Verification for Optimized FIN3

The predicted and measured performance of FIN3 is shown in Figures 6 and 7.  $C_{NFS}$  and  $x_{CP}/c_R$  are shown for  $M_\infty = 0.5$  and  $2.0$  and  $\delta = 0$  and  $20^\circ$  as a function of  $\alpha$ . The results for FIN3 are similar to FIN1. The comparisons of the measured and predicted  $C_{NFS}$  for

$\delta = 0^\circ$  are in good agreement for both Mach numbers. However, *OPTMIS* slightly overpredicts the normal force at  $\alpha = 20^\circ$ . *OVERFLOW* results are shown for  $M_\infty = 2.0$  and match the normal force well. The axial center-of-pressure location is also predicted well for the  $\delta = 0^\circ$  conditions, within 2% of  $c_R$ . The predicted results for  $\delta = 20^\circ$  are similar to those of FIN1 in terms of  $C_{NFS}$ . The predictions for axial center of pressure do not agree with experiment for  $\delta = 20^\circ$ . The reasons for the lack of agreement given above for FIN1 apply here also.

### Comparison of FIN1 and FIN3

A detailed comparison of experimental  $x_{CP}/c_R$  data for reference FIN1 and optimized FIN3, along with predicted results, are shown in Figure 8 for the design Mach numbers 0.5 and 2.0. Again, the design objective for FIN3 was to minimize axial center-of-pressure travel from subsonic to supersonic speeds. Measured and predicted results for FIN3 (optimized) and FIN1 (reference) are shown for  $\delta = 0^\circ$ . The axial center of pressure is plotted as a function of  $C_{NF}$  (based on base diameter). Predicted results are shown from the *OPTMIS*<sup>2</sup> code and the *OVERFLOW*<sup>22</sup> code. The experimental data, the results from the *OPTMIS* code, and the CFD results indicate that the optimized FIN3 has less center-of-pressure travel from subsonic to supersonic speeds and that the optimized fin has a flatter axial center-of-pressure variation with increasing  $C_{NF}$  as compared to the reference fin. For  $C_{NF} = 0.3$  FIN3 has 50% less center-of-pressure travel than FIN1. There is, in general, good agreement between the predictions and the experiment. FIN3 produces less normal force than FIN1 for the same angle of attack, due to the smaller fin area. However, the normal force can be increased by a higher angle of attack or fin deflection without adversely affecting center-of-pressure travel.

Figure 9 compares the FIN1 and FIN3 axial center-of-pressure location for all four test Mach numbers and for  $\delta = 0^\circ$  and  $20^\circ$ . The vertical axis ( $x_{CP}/c_R$ ) for both graphs in Figure 6 spans 0.32. For supersonic Mach numbers (1.5, 2.0, and 3.0), FIN3 shows only slight variations of  $x_{CP}/c_R$  with either  $\alpha$  or  $\delta$  compared to the reference FIN1.

### Results for Optimized FIN5 and Reference FIN6

The predicted and measured performance of the large span fins FIN5 and FIN6 are shown in Figure 10.  $C_{NFS}$  and  $x_{CP}/c_R$  are shown for  $M_\infty = 0.5$  and 2.0 for  $\delta = 0^\circ$  as a function of angle of attack. The comparisons of the measured and predicted  $C_{NFS}$  for  $\delta = 0^\circ$  are in good agreement for both Mach numbers. *OPTMIS* does not predict the stall characteristics for the  $M_\infty = 0.5$  flow condition. The axial center-of-pressure location is

predicted slightly aft of the experimental value for moderate angles of attack (unstalled), within 5% of  $c_R$ .

FIN5 was designed to have a reduced center-of-pressure travel from subsonic to supersonic speeds. The design flow conditions were:  $(M_\infty, \alpha) = (0.5, 2^\circ)$  and  $(2.0, 15^\circ)$ . Both fins have similar normal force characteristics. The optimized fin FIN5 delays stall and reaches a higher peak normal force than the reference fin at subsonic speeds. The axial center-of-pressure results for  $M_\infty = 0.5$  and 2.0 indicate that FIN5 has reduced center-of-pressure travel from subsonic to supersonic speed up to the onset of stall of the reference fin FIN6.

### Aeroelastic Fin Design

Aeroelastic design studies have been performed to improve missile fin performance through beneficial passive deformations of the fin structure under aerodynamic load. A description of the design and testing of an aeroelastic fin structure<sup>13</sup> used to demonstrate the potential of chordwise flexibility to control center-of-pressure location is described. This is followed by a recent study<sup>3</sup> aimed at using aeroelastically tailored composite fins.

In the earlier study,<sup>13</sup> an aeroelastic tailoring procedure was developed based on the SUPDL<sup>12,13</sup> code and a structural finite element code FEMOD.<sup>13</sup> The design procedure was successfully applied to a grooved aluminum lifting surface resulting in grooves in essentially the spanwise direction. The grooved aluminum trapezoidal fin is shown in Figure 11(a).  $C_{NFS}$  and  $x_{CP}/c_R$  are shown in Figure 11(b) and 11(c), respectively, for the flexible and rigid fins as a function of  $\alpha$  for  $M_\infty = 1.5, 2.5,$  and  $3.5$ . Predictions are designated TAILOR in Figure 11. The design objective was to shift  $x_{CP}/c_R$  forward to the maximum possible extent by varying the direction of the grooves. The design calculations indicated that  $x_{CP}/c_R$  could be shifted forward, without appreciable change in  $C_{NFS}$ , with grooves in a near spanwise direction. The experimental data shown in Figure 11 confirm this result.

The objective of the recent study<sup>3</sup> was to minimize the fin axial center-of-pressure travel over a Mach number range of 1.2 to 2.5 for  $\alpha = 5^\circ$ . The planform shape was fixed and the fin was undeflected. The design variables governing the fin structure are the fin thickness parameters at the fin root and the fin tip, and the principal stiffness axis orientation,  $\beta$ , of the composite fin lay-ups. A single orientation can be chosen, or the fin can be modeled as composed of up to three different layup orientation regions: the leading edge area of the fin, the middle portion of the fin, and the trailing edge region. The configuration modeled and the design variables governing the aeroelastic design are shown in

Figure 12. Details of the structural modeling of the composite layup and structural properties can be found in Reference 3. Structural displacement and stress constraints ensure that *realistic* fin structures are considered during the optimization process.

To start the optimization, a constant thickness fin was specified. The thickness distribution of the optimized fin is depicted in Figure 13. The principal structural axes for this fin are  $\beta_{LE} = 2.7^\circ$  for  $x/c_R \leq 3/8$  and  $\beta_{TE} = -48.3^\circ$  for  $x/c_R \geq 3/8$ . The deformation of the fin midplanes at  $M_\infty = 1.2$  and 2.5 are shown in Figure 14. A large deformation of the fin at the root chord leading edge is indicated. The normal force and axial center-of-pressure performance of the fin are shown in Table 1 and Figure 15. Figure 15 indicates that the optimized flexible fin maintains the normal force of the rigid fin. The space marching NEARZEUS<sup>23</sup> results shown in Figure 15 extends the normal force prediction to high Mach numbers. The reduced center-of-pressure travel is indicated in Figure 15 for the aeroelastic fin. NEARZEUS<sup>23</sup> predicts a similar forward shift of the center of pressure for the flexible fin.

Table 1.- Rigid and Optimized Flexible Performance

	$M_\infty$	$\alpha$	$C_{NFs}$	$x_{cp}/c_R$	$\Delta x_{cp}/c_R$
<b>Rigid</b>					
<b>OPTMIS</b>	1.2	5°	0.208	0.36	13.8%
<b>OPTMIS</b>	2.5	5°	0.168	0.5	
<b>Opt.</b>					
<b>OPTMIS</b>	1.2	5°	0.214	0.34	6.10%
<b>OPTMIS</b>	2.5	5°	0.168	0.4	
<b>Optimized fin <math>\Delta x_{cp}/c_R</math> reduced 56% vs. Rigid</b>					

The optimized fin has nearly the same normal force characteristics of the rigid fin but the center-of-pressure travel over the Mach number range is reduced 56%.

### CONCLUSIONS

An optimization-based design tool for missile fin and configurations design and analysis has been developed. The design capabilities of the method for fin planform optimization have been verified with CFD calculations and with a wind tunnel test. Significant improvements to center-of-pressure travel, and hence hinge moments, can be obtained through planform optimization. Initial studies of aeroelastic fin structures indicate that significant improvements to fin performance can be obtained through the use of flexible structures. The speed and multidisciplinary capabilities of the method make it an excellent tool for preliminary design. Both

conventional circular body and unconventional noncircular body configurations can be designed and analyzed.

### ACKNOWLEDGEMENTS

The authors would like to thank Dr. Andy Sullivan and Mr. Fred Davis of the Air Force Research Labs, Flight Vehicle Branch WL/MNAV, at Eglin AFB for their support of this work under Air Force Contract F08630-94-C-0054, also, Dr. Craig Porter from NAWCWPNS, China Lake for sponsoring the aeroelastic fin design effort under Navy Contract N68936-97-C-0152. Dr. Samuel McIntosh, McIntosh Structural Dynamics, Palo Alto, CA, was responsible for the structural modeling described.

### REFERENCES

1. Lesieutre, D.J., Dillenius, M.F.E., and Lesieutre, T.O., "Optimal Aerodynamic Design of Advanced Missile Configurations With Geometric and Structural Constraints," NEAR TR 520, September 1997.
2. Lesieutre, D.J., Dillenius, M.F.E., and Lesieutre, T.O., "Missile Fin Planform Optimization For Improved Performance," Presented at NATO RTA/AVT Spring 1998 Symposium on Missile Aerodynamics, Paper 4, Sorrento, Italy, May 1998.
3. Lesieutre, D.J., Dillenius, M.F.E., Love, J.F., and Perkins, S.C., Jr., "Control of Hinge Moment by Tailoring Fin Structure And Planform," NEAR TR 530, December 1997.
4. Lacau, R.G., "A Survey of Missile Aerodynamics," *in* Proceedings, NEAR Conference on Missile Aerodynamics, October 1988.
5. Briggs, M.M., "Systematic Tactical Missile Design," *in* Tactical Missile Aerodynamics: General Topics, 141, 3, Progress in Astronautics and Aeronautics, AIAA, 1991.
6. Nielsen, J.N., "Missile Aerodynamics," New York, McGraw-Hill, 1960; Reprint, Mountain View, CA, Nielsen Engineering & Research, 1988.
7. Lesieutre, D.J. and Dillenius, M.F.E., "Chordwise and Spanwise Centers of Pressure of Missile Control Fins," AGARD CP 493 Paper 30, April 1990.
8. Allen, J.M., Shaw, D.S., and Sawyer, W.C., "Remote Control Missile Model Test," AGARD CP 451 Paper 17, May 1988.
9. Powell, M.J.D., "An Efficient Method for Finding the Minimum of a Function of Several Variables Without Calculating Derivatives," *Computation Journal*, 7, 1964, pp 155-162.
10. Sargent, R.W.H., "Minimization without Constraints," *in* "Optimization and Design," Avriel, M., Rijckaert, M.J., and Wilde, D.J., (Eds.), Englewood Cliffs, New Jersey, Prentice-Hall, 1973.

11. Lesieutre, D.J., Dillenius, M.F.E., and Whittaker, C.H., "Program SUBSAL and Modified Subsonic Store Separation Program for Calculating NASTRAN Forces Acting on Missiles Attached to Subsonic Aircraft," NAWCWPNS TM 7319, May 1992.
12. Dillenius, M.F.E., Perkins, S.C., Jr., and Lesieutre, D.J., "Modified NWCDM--NSTRN and Supersonic Store Separation Programs for Calculating NASTRAN Forces Acting on Missiles Attached to Supersonic Aircraft," Naval Air Warfare Center Report NWC TP6834, September 1987.
13. Dillenius, M.F.E., Canning, T.N., Lesieutre, T.O., and McIntosh, S.C., "Aeroelastic Tailoring Procedure to Optimize Missile Fin Center of Pressure Location," AIAA Paper 92-0080, January 1992.
14. Hegedus, M.C. and Dillenius, M.F.E., "VTXCHN: Prediction Method For Subsonic Aerodynamics and Vortex Formation on Smooth and Chined Forebodies at High Alpha," AIAA Paper 97-0041, January 1997.
15. Fiacco, A.V. and McCormick, G.P., "Nonlinear Programming," New York, John Wiley & Sons, Inc., 1968.
16. Carmichael, R.L. and Woodward, F.A., "An Integrated Approach to the Analysis and Design of Wings and Wing-Body Combinations in Supersonic Flow," NASA TN D-3685, October 1966.
17. Dillenius, M.F.E., "Program LRCMD2, Improved Aerodynamic Prediction Program for Supersonic Canard-Tail Missiles With Axisymmetric Bodies," NASA CR 3883, April 1985.
18. Polhamus, E.C., "Prediction of Vortex-Lift Characteristics Based on a Leading-Edge Suction Analogy," J.Aircraft, 8, April 1971, pp 193-199.
19. Dillenius, M.F.E. and Perkins, S.C., Jr., "Computer Program AMICDM, Aerodynamic Prediction Program for Supersonic Army Type Missile Configurations with Axisymmetric Bodies," U.S. Army Missile Command Technical Report RD-CR-84-15, June 1984.
20. Przemieniecki, J.S., "Theory of Matrix Structural Analysis," New York, McGraw-Hill, 1968.
21. McIntosh, S.C., "Optimization and Tailoring of Lifting Surfaces with Displacement, Frequency, and Flutter Performance Requirements," NWC TP 6648, April 1987.
22. Buning, P.G., Chan, W.M., et al., "OVERFLOW User's Manual - Version 1.6be" unpublished NASA document, February 1996.
23. Perkins, S.C., Jr., Wardlaw, A.W., Jr., Priolo, F., and Baltakis, F., "NEARZEUS User's Manual, Vol. I: Operational Instructions, Vol. II: Sample Cases, Vol. III: Boundary Layer Code ZEUSBL," NEAR TR 459, May 1994.

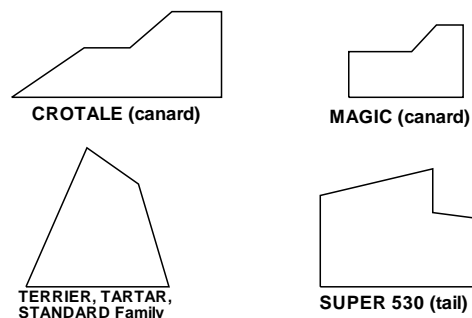


Figure 1.- Control surfaces with limited center-of-pressure shifts.<sup>4</sup>

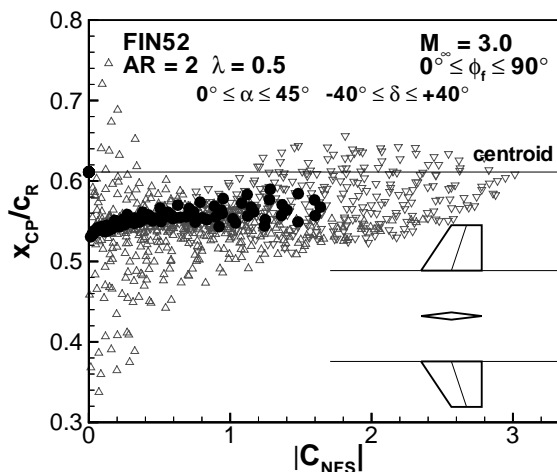


Figure 2.- Triservice FIN52,  $x_{CP}/c_R$  as function of  $C_{NFS}$  at  $M_\infty = 3.0$  for  $0^\circ \leq \alpha \leq 45^\circ$ ,  $0^\circ \leq \phi_f \leq 90^\circ$  and  $-40^\circ \leq \delta \leq +40^\circ$  (solid symbols are  $\delta = 0^\circ$ ).

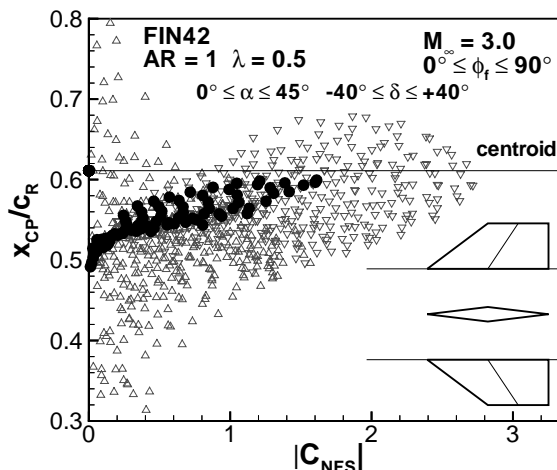


Figure 3.- Triservice FIN42,  $x_{CP}/c_R$  as function of  $C_{NFS}$  at  $M_\infty = 3.0$  for  $0^\circ \leq \alpha \leq 45^\circ$ ,  $0^\circ \leq \phi_f \leq 90^\circ$  and  $-40^\circ \leq \delta \leq +40^\circ$  (solid symbols are  $\delta = 0^\circ$ ).

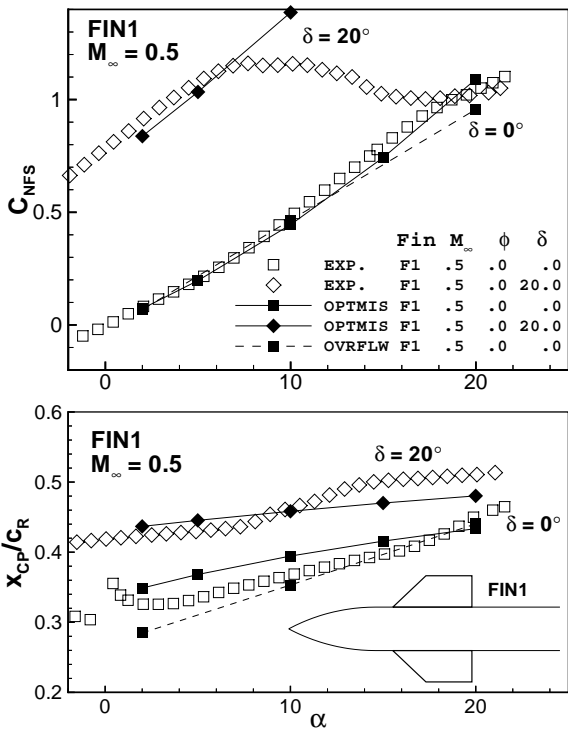


Figure 4.- Comparison of measured and predicted  $C_{NFS}$  and  $x_{CP}/c_R$  for FIN1 at  $M_\infty = 0.5$ .

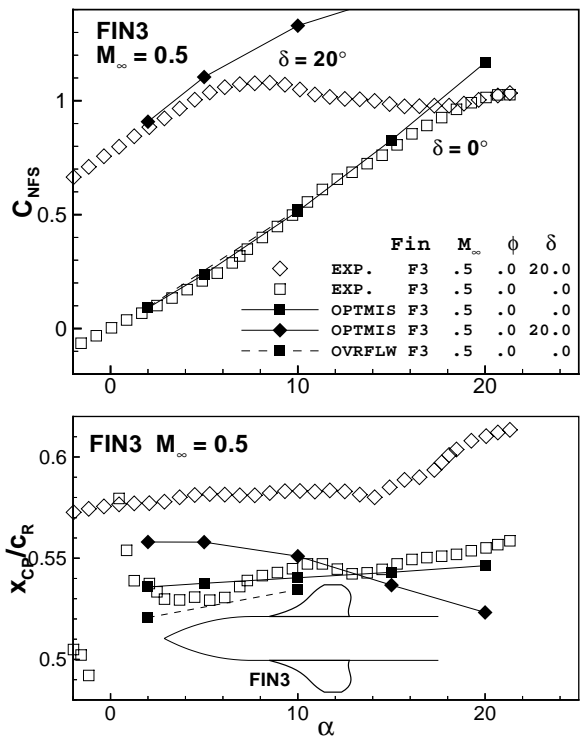


Figure 6.- Comparison of measured and predicted  $C_{NFS}$  and  $x_{CP}/c_R$  for FIN3 at  $M_\infty = 0.5$ .

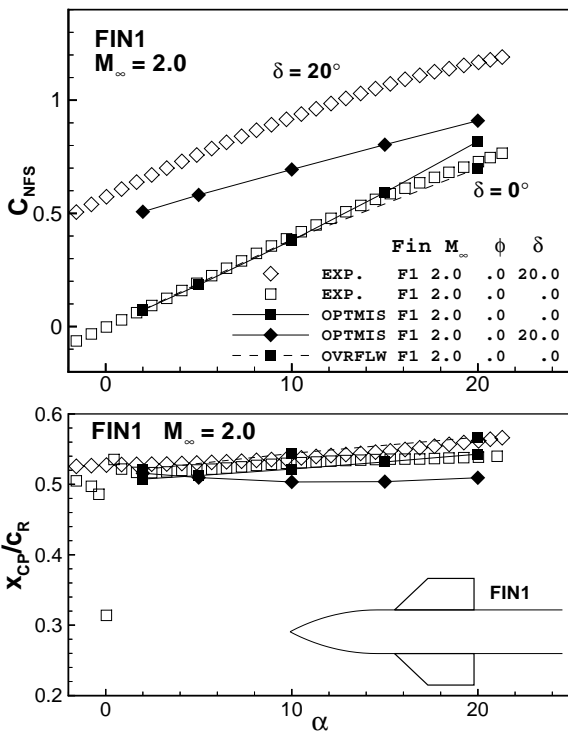


Figure 5.- Comparison of measured and predicted  $C_{NFS}$  and  $x_{CP}/c_R$  for FIN1 at  $M_\infty = 2.0$ .

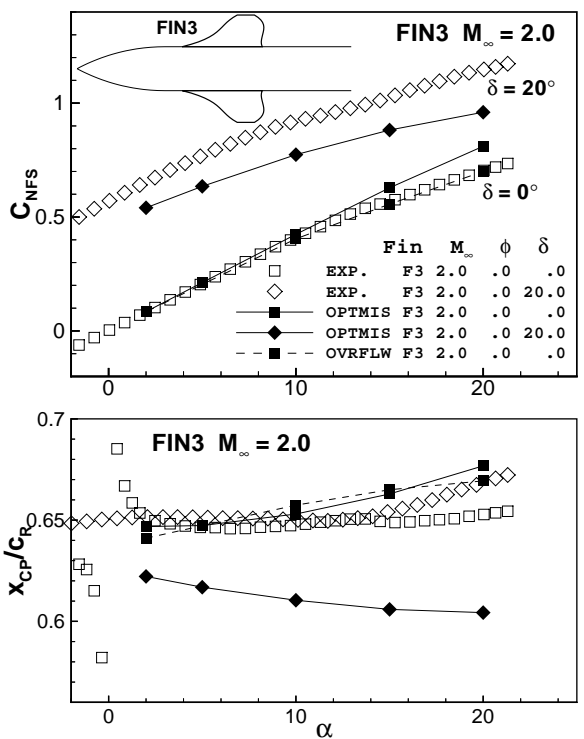


Figure 7.- Comparison of measured and predicted  $C_{NFS}$  and  $x_{CP}/c_R$  for FIN3 at  $M_\infty = 2.0$ .

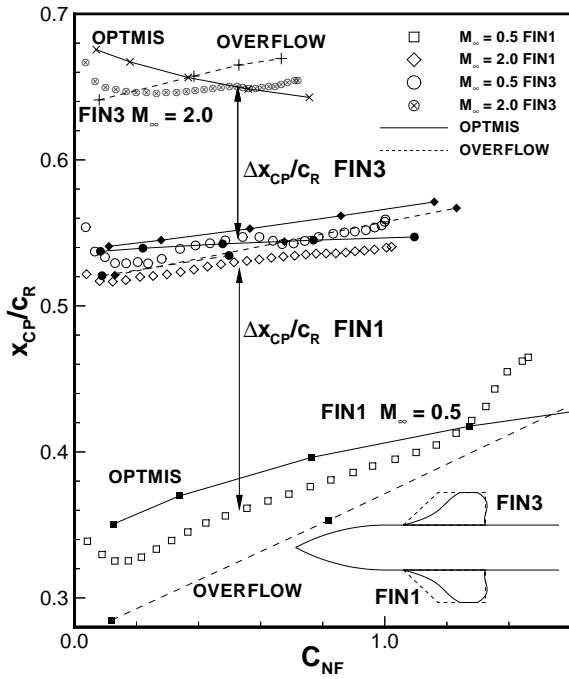


Figure 8.- Comparison of measured and predicted  $x_{CP}/c_R$  for reference fin FIN1 and optimized fin FIN3,  $M_\infty = 0.5$  and 2.0.

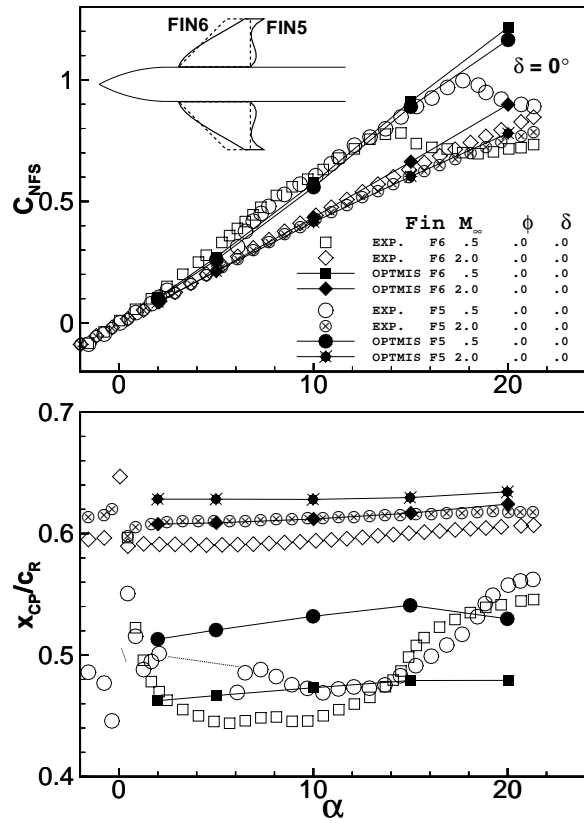


Figure 10.- Comparison of measured and predicted  $C_{NFS}$  and  $x_{CP}/c_R$  for FIN5 and FIN6 at  $M_\infty = 0.5$  and 2.0.

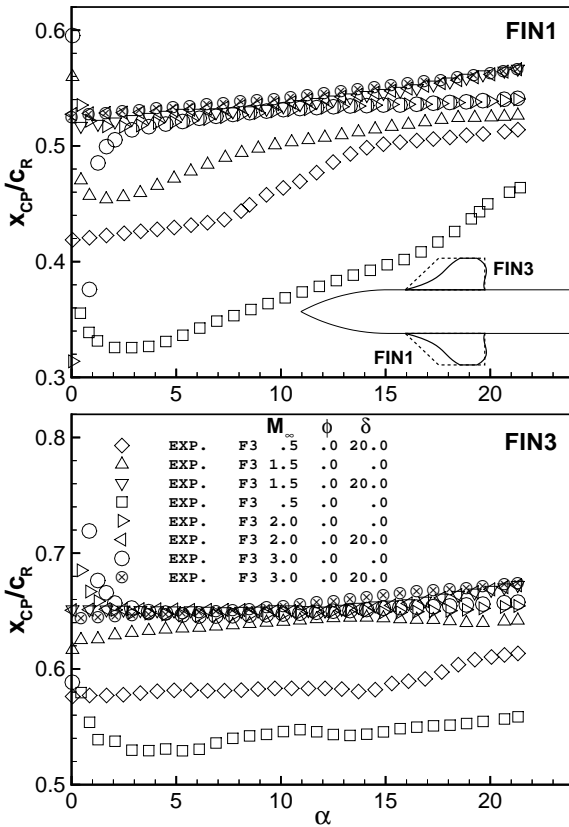
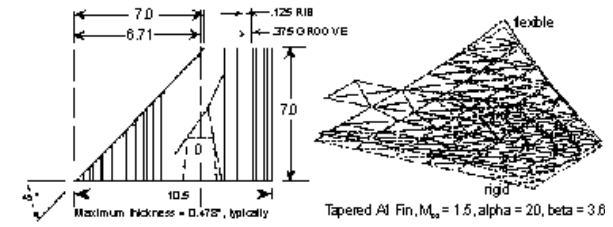
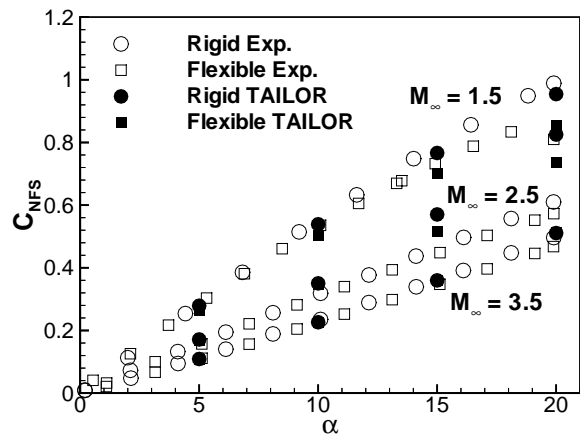


Figure 9.- Measured  $x_{CP}/c_R$  for reference FIN1 and optimized FIN3,  $M_\infty = 0.5, 1.5, 2.0$  and 3.0;  $\delta = 0^\circ$  and  $20^\circ$ .



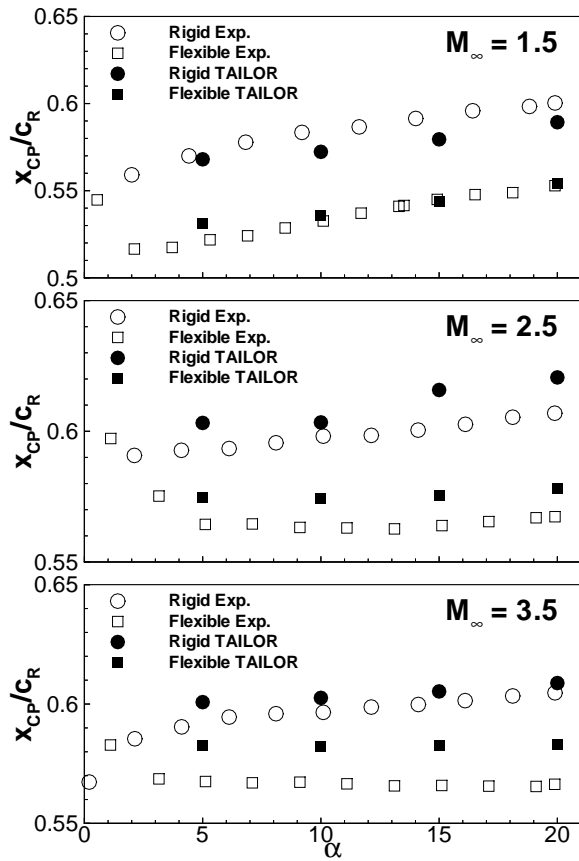
(a) Grooved flexible fin.

Figure 11.- Performance of rigid and grooved flexible fins.



(b) Variation of  $C_{NFS}$  with angle of attack.

Figure 11.- Continued.



(c) Variation of  $x_{CP}/c_R$  with angle of attack.  
Figure 11.- Concluded.

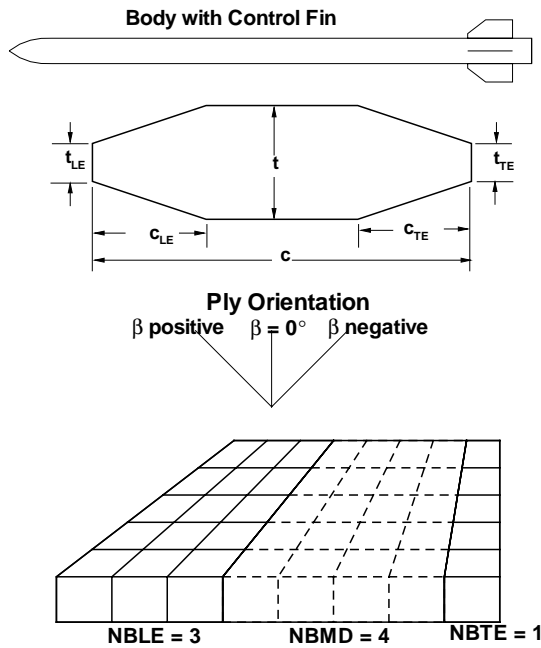


Figure 12.- Configuration and design variables used for the aeroelastic fin design study.

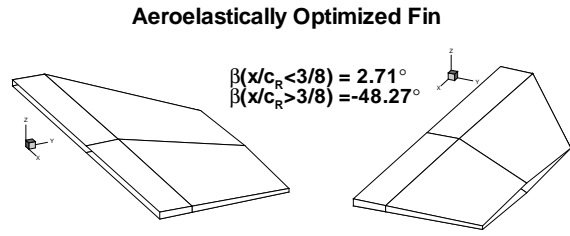


Figure 13.- Optimized aeroelastic fin thickness.

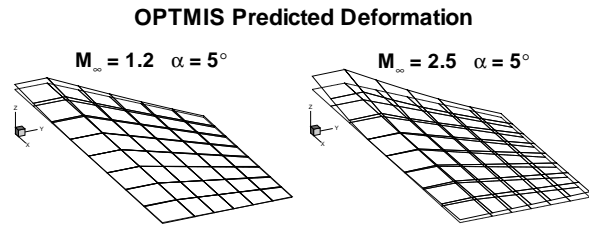


Figure 14.- Predicted aeroelastic deformations.

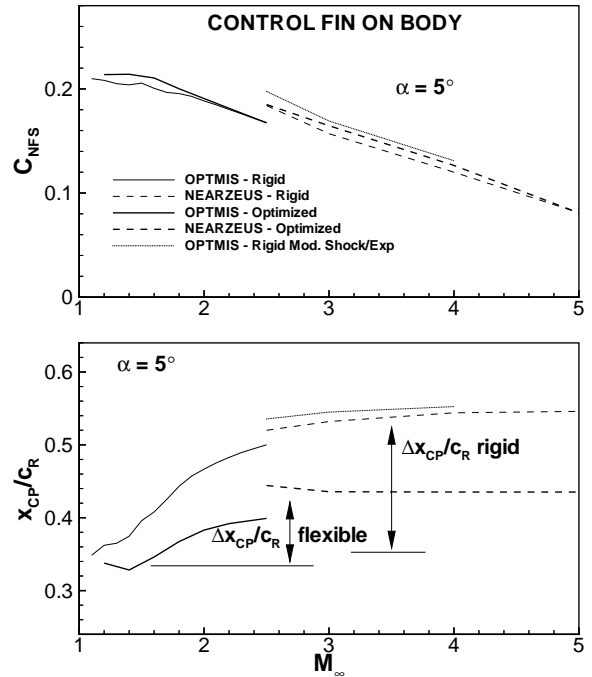


Figure 15.- Comparison of rigid and flexible fin performance.